Vol. 8, No. 1, February 2024, pp. 72-79

Current Optics and Photonics

Regular Paper

Diffractive Alignment of Dual Display Panels

Shin-Woong Park[1], Junghwan Park[2], and Hwi Kim[2]*

[1]*Center for Advanced Photovoltaic Materials (CAPM), Korea University, Sejong 30029, Korea*
[2]*Department of Electronics and Information Engineering, Korea University, Sejong 30029, Korea*

(Received October 5, 2023 : revised November 20, 2023 : accepted November 20, 2023)

Recent flat-panel displays have become increasingly complicated to facilitate multiple display functions. In particular, the form of multilayered architectures for next-generation displays makes precise three-dimensional alignment of multiple panels a challenge. In this paper, a diffractive optical alignment marker is proposed to address the problem of three-dimensional alignment of distant dual panels beyond the depth-of-focus of a vision camera. The diffractive marker is effective to analyze the positional correlation of distant dual panels. The possibility of diffractive alignment in multilayer display fabrication is testified with numerical simulation and a proof-of-concept experiment.

Keywords : Binary diffractive optical element (DOE), Depth-of focus, Diffractive alignment, Dual display panels, Multilayered display technology
OCIS codes : (090.1970) Diffractive optics; (120.2040) Displays

I. INTRODUCTION

In recent decades, multilayered display technology has rapidly advanced for multifunctional flat-panel display (FPD) products [1, 2]. Commercialized FPD products now offer a multi-functional display architecture by including additional layers such as a touch sensor sheet [3], a lenticular lens sheet [4, 5], and a film-patterned retarder (FPR) [6, 7]. Along with this trend, precise panel alignment has become a crucial issue in display manufacturing [8–15]. Precise alignment and clear bonding of the multiple panels is essential to achieve the intended performance of the multilayered displays [16–20]. In particular, the dual-layer FPD structure has recently been considered a candidate to achieve complex spatial light modulation (SLM) in the field of wave optics [21]. In order to modulate the wavefront of light more systematically, multilayer architectures with an extra degree of freedom are employed in SLMs. However, the pixel-to-pixel interconnection of multiple panels to achieve high efficiency in complex modulation is considered a challenge.

There are plural alignment approaches. One approach is the visual alignment of electrode patterns positioned at the same coordinates on the lower and upper panels [22]. Another approach involves irradiating the alignment film with ultraviolet rays whenever a panel layer is attached to the display [23] Recently, the use of photographic markers on each panel to align multiple panels using a vision camera has become popular [24]. However, a conventional vision camera cannot capture the in-focus images of two axially distant markers on the layered panels at the same time when the distance between the two panel plates surpasses the depth-of-focus (DOF) range of the vision camera. This makes it difficult to achieve accurate three-dimensional alignment of multiple panels in the conventional vision-based alignment system.

In this paper, the problem of alignment of axially distant dual panels is investigated. To overcome the DOF limitation in axial alignment, we propose a diffractive axial alignment method using a diffractive marker. The central idea is that a binary diffractive optical element (DOE) inscribed on the lower panel generates an in-focus marker image on

*Corresponding author: hwikim@korea.ac.kr, ORCID 0000-0002-4283-8982
Color versions of one or more of the figures in this paper are available online.

pISSN: 2508-7266 / eISSN: 2508-7274 https://doi.org/10.3807/COPP.2024.8.1.72

the upper panel. A vision camera with a focus on the upper panel can monitor the in-focus diffractive marker image of the lower panel and estimate the degree of alignment of two panels by comparing it to the normal marker image of the upper panel. The algorithm for estimating the relative lateral shift and rotation (counterclockwise direction) between two distant glass panels using the proposed diffractive marker presents proof-of-concept experimental results. For this, a binary DOE pattern is designed to be compatible with conventional glass-based display fabrication infrastructure [25–29].

II. DESIGN OF DIFFRACTIVE ALIGNMENT SYSTEM

2.1. Wave Optic Modeling of the Diffractive Alignment Process

Figure 1(a) presents the schematics of the proposed diffractive alignment system for two distant display panels. Assume that a lower panel is placed on the x-y plane (z = 0) and the upper panel is a finite distance above the lower panel, which is supposed to be orthogonal to the z-axis for simplicity. The inter-distance of two panels is assumed to be longer than the vision camera's DOF. A binary DOE pattern is designed [30] and fabricated on the lower panel to generate an in-focus diffraction marker image on the upper panel. The upper panel is engraved with a normal reference marker. The design is intended to enable the vision camera to monitor the normal reference marker of the upper panel and the diffractive marker of the lower panel at the same time. Thus, the camera focus of the vision camera is tuned to the surface of the upper panel. A divergent light wave illuminates the DOE and the diffractive field propagates toward the positive z-direction to form a diffraction marker image. The complex light field at $z = 0$ is denoted by $U(x, y; z = 0)$. The optical field distribution in the upper panel can be represented by the angular spectrum integral [26, 31],

$$U(x,y;z=z') = \int_{-\infty}^{\infty}\int_{-\infty}^{\infty} A(\alpha,\beta)\exp\left(j2\pi(\alpha x+\beta y+\gamma z)\right)d\alpha d\beta, \quad (1)$$

where $A(\alpha, \beta)$ is the angular spectrum of $U(x, y; z = 0)$ given

$$A(\alpha,\beta) = \int_{-\infty}^{\infty}\int_{-\infty}^{\infty} U(x,y;z=0)\exp\left(-j2\pi(\alpha x+\beta y)\right)dxdy. \quad (2)$$

To reduce the DC and conjugate noise of the binary diffractive marker in the upper panel, a divergent light source is employed, which spreads out the DC and conjugate terms and focuses only the signal component on the target region. The DOE should be optimized to synthesize the diffractive marker image under the divergent light source [31].

2.2. Design of Diffractive Optical Elements

In the registration and alignment process of two panels, two-step pre-processing illumination modes are needed, which is described in section 2.3. To design diffractive markers, the iterative Fourier transform algorithm (IFTA)

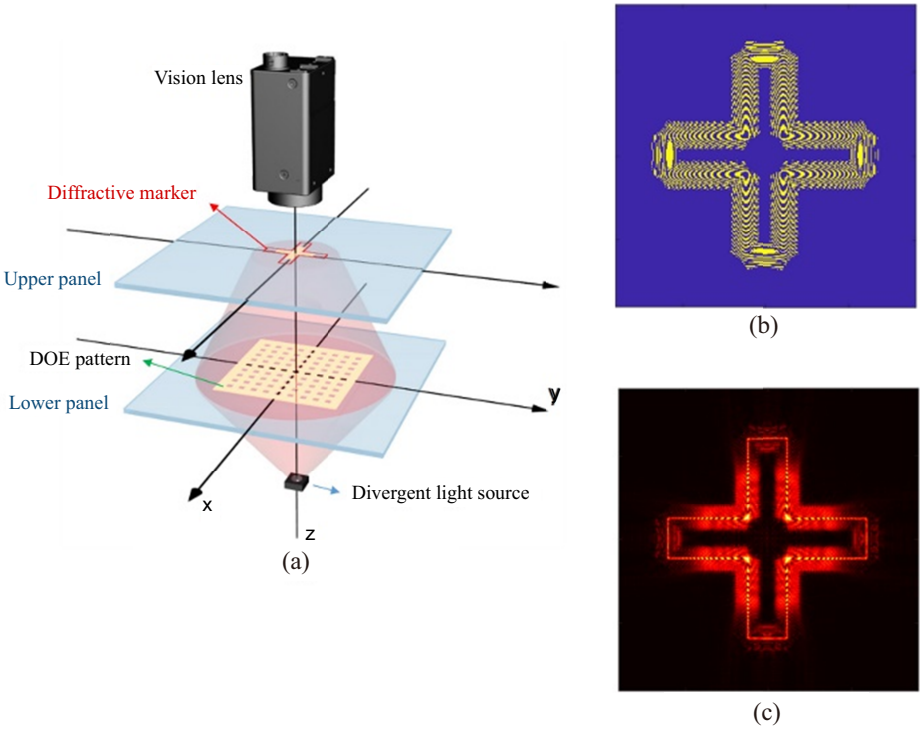

FIG. 1. Diffractive alignment process. (a) Diffractive alignment system of two axially distant panels, (b) designed binary diffractive optical element (DOE) marker pattern, and (c) diffractive marker image observed in the upper panel.

between $U(x, y; z = 0)$ and $U(x, y; z = z')$ is implemented based on the angular spectrum method (ASM) [32, 33]. In the ASM-based IFTA, a binary amplitude DOE is constrained to meet the minimum feature size (MFS) of the glass-based display fabrication infrastructure, which is supposed to be 1.5 μm. Since the Cu-patterning fabrication process with a minimum pitch of 3 μm is used to fabricate the experiment sample, the binary DOE pattern was designed with a resolution of 601 × 601 and a pixel pitch of 3 μm, as shown in Fig. 1(b).

In the numerical simulation of the diffractive marker formation process, a divergent light wave with a wavelength of 633 nm is incident to the DOE, and the diffractive light wave propagates through a 548-μm-thick air layer and a 280-μm-thick top glass layer to form a diffractive marker on the top surface of the upper panel. The in-focus diffraction image of the designed DOE is presented in Fig. 1(c). This result satisfies the MFS constraint. It is seen that a highly focused thin-line cross edge image is obtained, which can be easily analyzed by the conventional edge-detection algorithm.

2.3. Image Registration and Affine Transform

To estimate the alignment of the upper and lower panel diffractive markers separately, a two-step illumination sequence is employed. In the first illumination mode, only the top marker is detected by disabling the diffractive marker by using an incoherent extended light source that does not form any patterns while penetrating the DOE of the lower panel. While the diffractive marker in the lower panel is not visible, the vision system performs the edge detection of the upper panel marker. For the second mode, a divergent point light source was used for the edge detection of the holographic marker on the lower panel. This is because the divergent point light source can penetrate the DOE of the lower layer and form a holographic marker on the upper panel. The first illumination mode and the edge detection result of the upper marker are shown in Figs. 2(a)–2(c). The simulation assumes that the upper panel deviates 50 μm in the x-axis direction and 20 μm in the y-axis direction, and rotates by 3° in the counterclockwise direction from the reference position. The task of the second illumination mode of Fig. 2(d) is the recognition of the diffractive marker pattern that indicates the position of the lower panel. The sharp crossed pattern offered by the DOE is overlapped with the upper panel marker as shown in Fig. 2(e). Since the upper panel marker pattern is detected at the first illumination mode, the single image of the diffractive marker pattern of Fig. 2(f) can be easily acquired by edge detection and the sequential subtraction of the upper panel marker pattern.

To estimate the degree of the alignment of the lower and upper markers, a 2D affine matrix is defined. The 2D affine

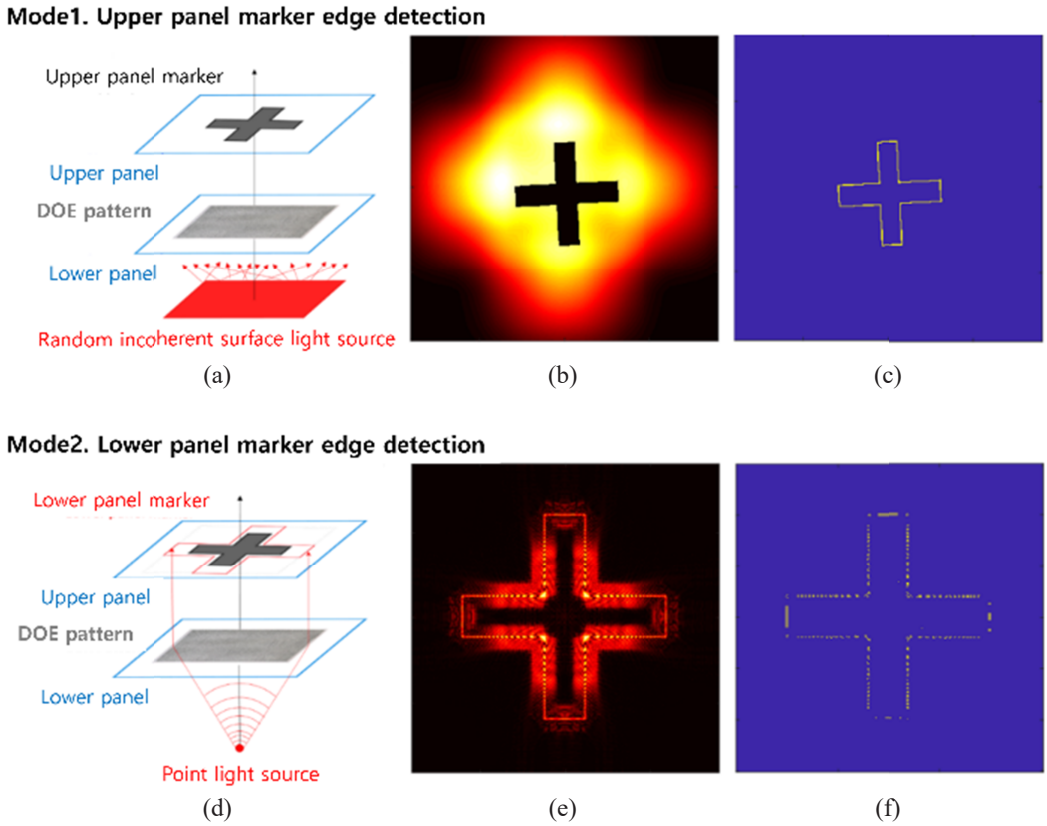

FIG. 2. Two sequential illumination modes for detecting (a) the upper and (d) lower markers. Simulation results for the first illumination mode: (b) vision camera observation image and (c) its edge detection image. Simulation results for the second illumination mode: (e) vision camera observation image and (f) its edge detection image.

matrix models the relative positional deviation between the two marker images by the form,

$$A = \begin{pmatrix} \cos\theta & -\sin\theta & 0 \\ \sin\theta & \cos\theta & 0 \\ d_x & d_y & 1 \end{pmatrix}, \quad (3)$$

where θ represents the rotation angle and d_x and d_y specify the displacement of two images along the x- and y-axes in pixels. Through the registration of the upper and lower markers, the 2D affine matrix is calculated and the information for the lateral shift and rotation is extracted from this matrix.

Figure 3(a) illustrates the estimation process for the relative shift and rotation of two panels using the affine matrix model. Figures 3(b) and 3(c) show the separate extraction

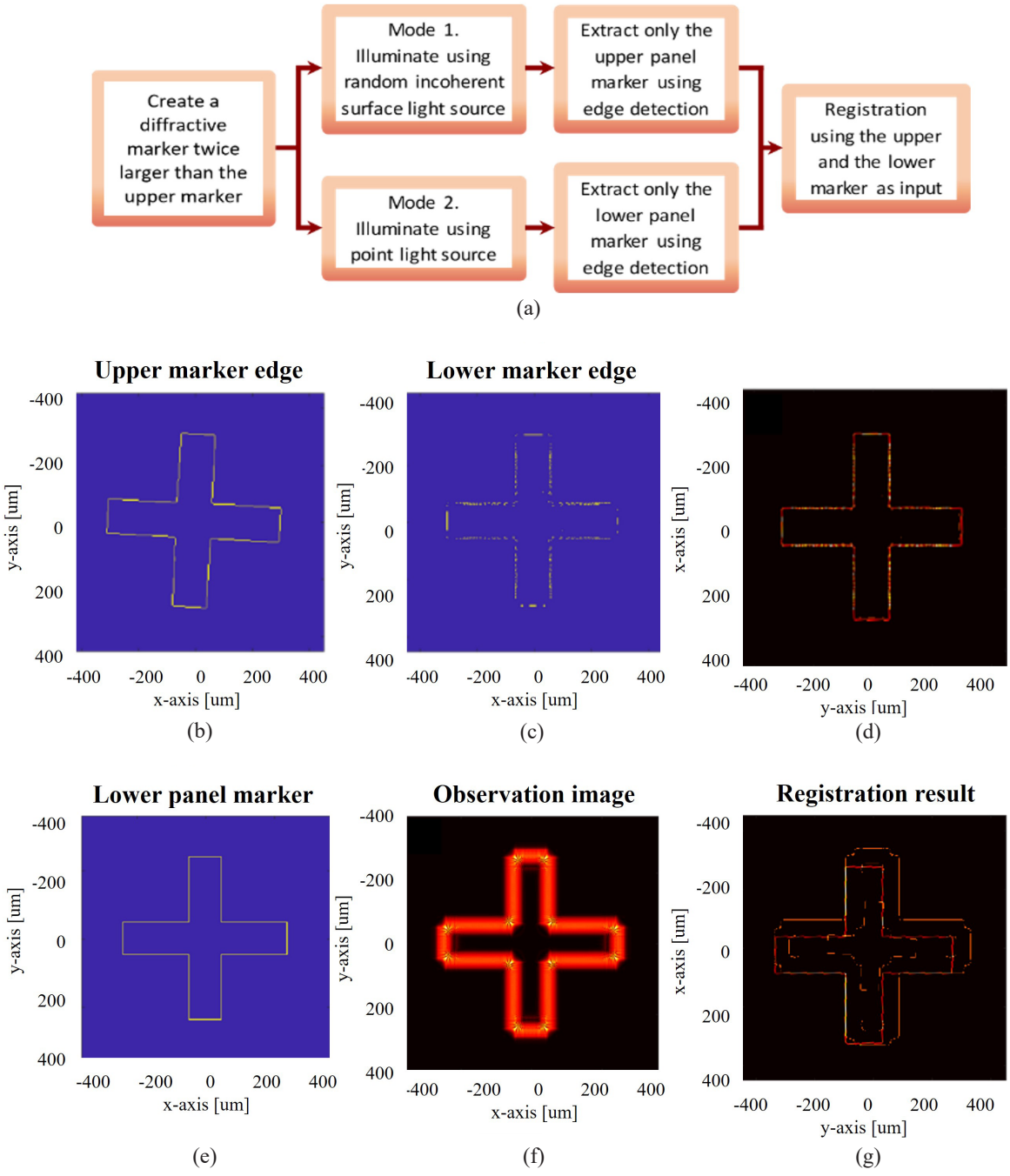

FIG. 3. Registration for panel markers. (a) Flow chart for the lateral deviation estimation using the affine image registration algorithm. The edge detection images of (b) upper and (c) lower panel markers, and (d) the image registration result. (e) Traditional 2D marker on the lower panel and (f) its observed image taken by the vision camera with a focus tuned to the upper panel. (g) The false registration results of the defocused lower marker image and the upper marker.

of the upper and lower panel markers. The affine matrix transforms the upper marker image to the lower marker image to constitute an overlapping image as in Fig. 3(d). The affine matrix of Eq. (3) is obtained for the simulation data of Figs. 3(b)–3(d) as

$$A = \begin{pmatrix} 0.9987 & -0.05143 & 0 \\ 0.05143 & 0.9987 & 0 \\ -12.86 & -7.320 & 1 \end{pmatrix}. \quad (4)$$

The alignment conditions, such as the lateral shift and rotation angle of the top panel, from the affine matrix are compared with the simulated true values to check the reliability of the algorithm. The components **A**(1, 1), **A**(1, 2), **A**(2, 1), and **A**(2, 2) represent the 2 × 2 rotation matrix, then the relative rotation angle can be obtained by taking the arccosine value of the matrix element. The components **A**(3, 1) and **A**(3, 2) indicate the relative shift in the *x*- and *y*-coordinates, respectively, in pixels. The distance of movement in the *x*- and *y*-directions is calculated by multiplying

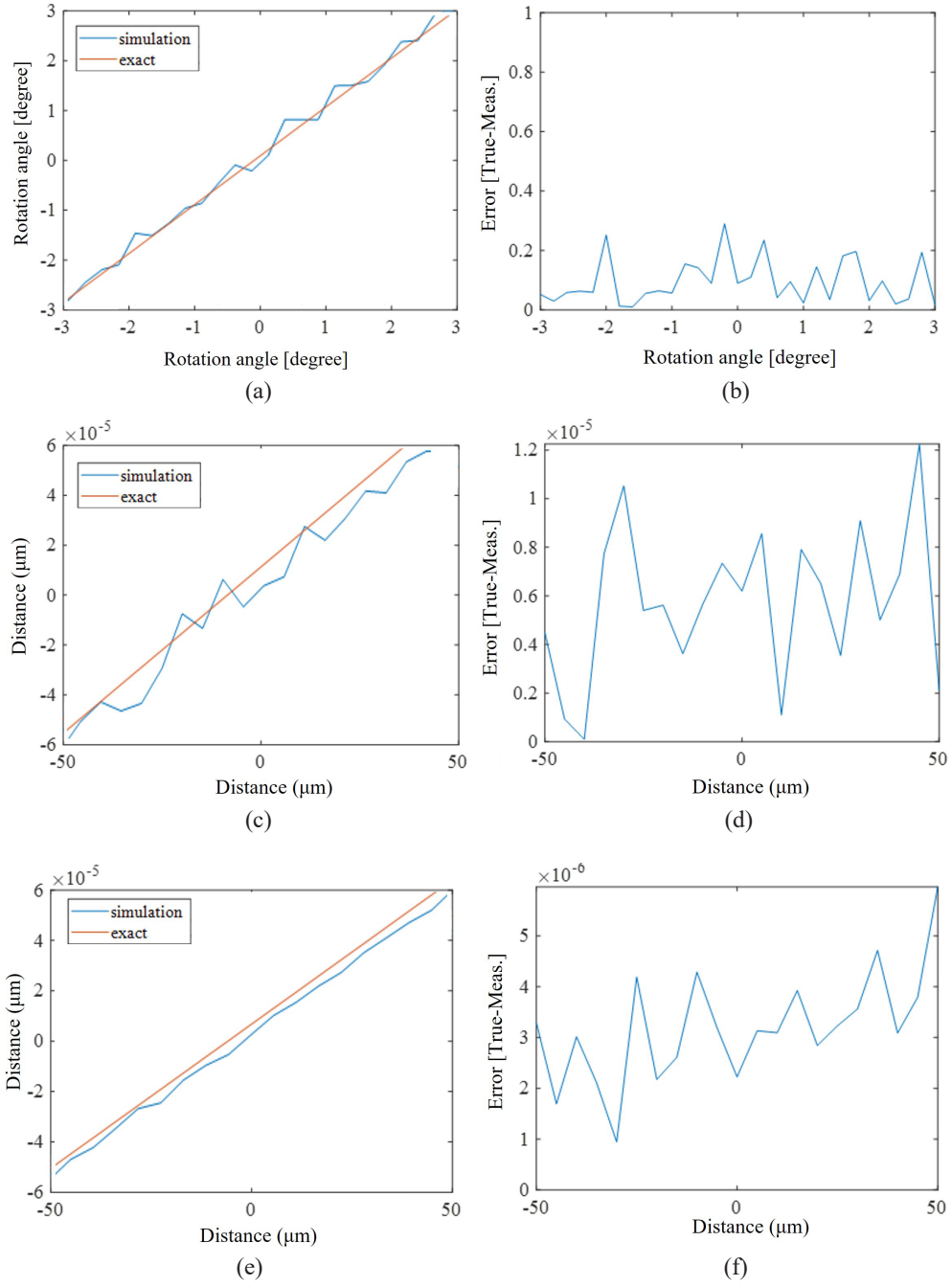

FIG. 4. Comparative graphs of the true and estimated values of (a) rotation angle, (c) *x*-directional lateral shift, (e) *y*-directional lateral shift. The error values for (a), (c), and (e) are plotted in (b), (d), and (f), respectively.

these by the pixel pitch to obtain the shift error.

The proposed technique is compared with a traditional alignment method employing conventional non-diffractive markers (*i.e.*, non-diffractive) in Figs. 3(e)–3(g). A hollow cross pattern is taken as the target marker image [Fig. 3(e)]. The vision camera with a focus tuned to the upper panel perceives the defocused image of the lower panel marker [Fig. 3(f)]. Because of the defocusing effect, the affine matrix analysis is degraded due to the image registration failure [Fig. 3(g)]. Figure 4(a) compares the simulation

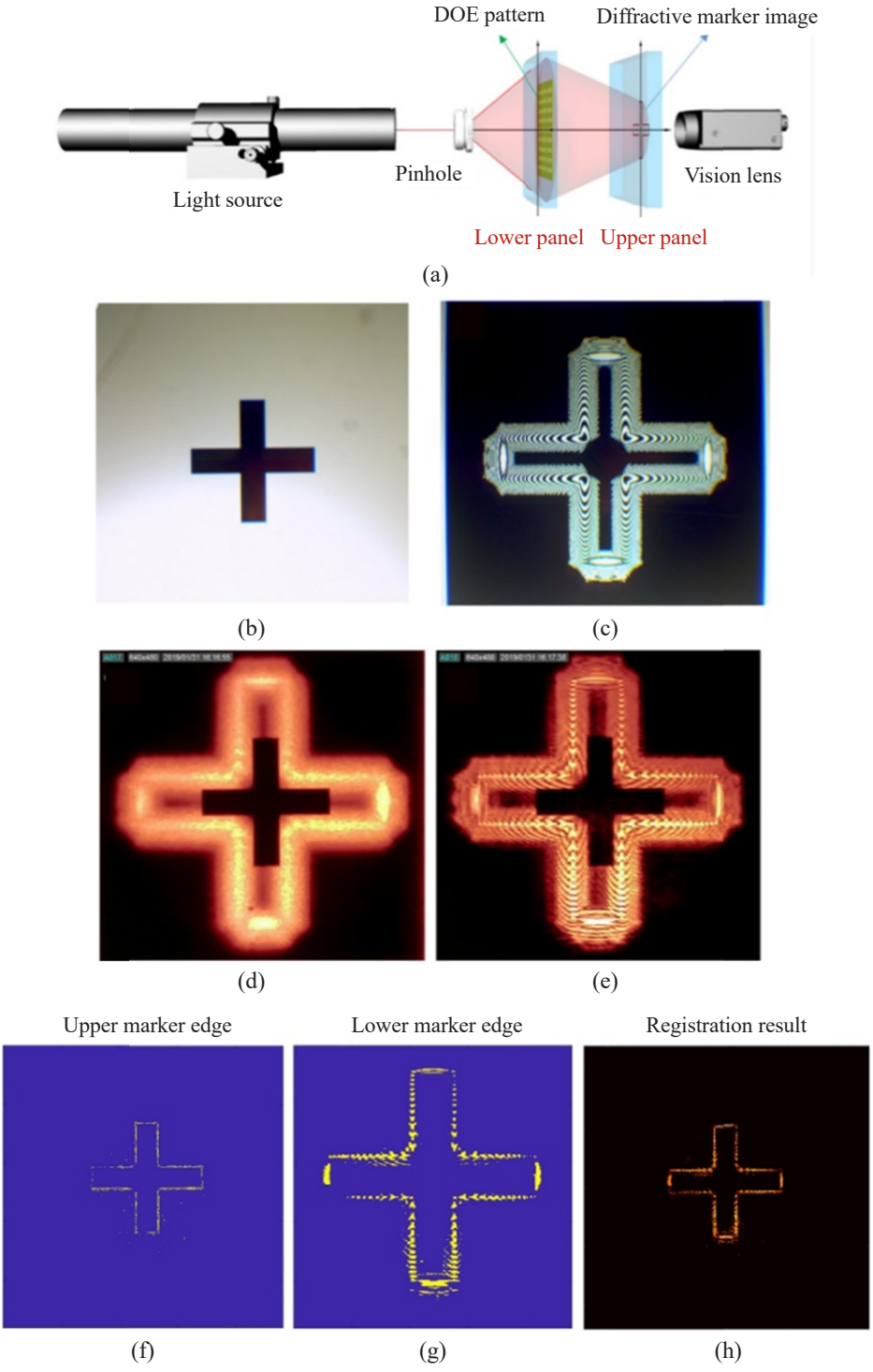

FIG. 5. Experimental results for diffractive alignment. (a) Experimental setup of the diffractive alignment, (b) upper marker pattern (6 mm × 6 mm), (c) lower DOE marker pattern (18 mm × 18 mm), (d) observation image of the upper marker in the first illumination mode, and (e) observation image of the lower diffractive marker in the second illumination mode. Edge detection results of (f) the upper marker, (g) the lower diffractive marker, and (h) the registration results of two markers.

results with the true values with an increase in the rotation angle of the top panel at intervals of 0.2° from −3° to 3°. In Fig. 4(b), the error between the two values is plotted with respect to the rotation angle, in which the maximum and the average error values are 0.290° and 0.156°, respectively. The accuracy can be further improved by employing a smaller pixel pitch or a higher resolution. Figures 4(c) and 4(e) present the simulation data comparing the true and estimated values for the lateral shift of the upper panel from −50 μm to 50 μm in the *x*-axis and *y*-axis directions, respectively. Figures 4(d) and 4(f) display the error between the true value and estimated value for the *x*- and *y*-directional shifts, respectively. In this simulation, a shift error up to 12 μm is observed; However, the accuracy can be improved if the DOE pixel pitch is further reduced and the resolution is made larger.

III. EXPERIMENTAL RESULTS

To experimentally verify the diffractive alignment method, we fabricated a binary DOE marker and conducted an alignment experiment. The experimental setup and the fabricated DOE are presented in Fig. 5(a). The focus of the camera vision is tuned to the top surface of the upper panel with a distance of 75 mm. A divergent light source with a wavelength of 633 nm filtered by a pinhole with a diameter of 50 μm illuminates the backside of the DOE on the lower panel. The thickness of the glass panels is 500 μm, and the distance between the upper and lower panel markers is 550 μm. The fabricated upper and lower markers are presented in Figs. 5(b) and 5(c), respectively. The pattern pixel pitch is 3 μm, and the resolution is set to 2,001 × 2,001 for the upper panel and 6,001 × 6,001 for the lower DOE. The DOE domain of the lower panel is designed to be three times as large as the upper panel marker. Figure 5(d) presents an observation image for the upper panel marker using an extended incoherent surface light source (illumination mode 1), while Fig. 5(e) shows an observation image for the lower panel diffractive marker using a divergent light source aperture by the 50 μm pinhole (illumination mode 2). Figures 5(f) and 5(g) show the edge detection results of the upper marker and lower marker, respectively, and the completed registration result of two images is shown in Fig. 5(h). The affine matrix for the experimental result is obtained by

$$\boldsymbol{A} = \begin{pmatrix} 1.00 & 0.00509 & 0.00000 \\ -0.00509 & 1.00 & 0.00000 \\ -14.0 & 6.47 & 1.00 \end{pmatrix}. \quad (5)$$

From the resulting affine 2D matrix, it can be seen that the markers on the upper and lower panels moved −14.4 and 6.47 pixels in the *x*- and *y*-directions, which translates to lateral movement of −228 μm and 102 μm in the *x*- and *y*-directions. The accuracy of the lateral shift of the affine matrix registration algorithm is at a one-pixel or sub-pixel level. Also, it is estimated that the upper and lower panels are relatively rotated by 0.292°, although the lateral shift is quite large in this experiment.

In addition to the lateral shift and relative rotation analysis demonstrated in this work, we can further extend our proposed method to measure and compensate for the three-dimensional tilting factor leading to non-parallel deviation of the panel, which still remains a challenging problem in the display manufacturing process. If the short DOF vision camera and the diffractive alignment technique are combined and the defocusing effect of the diffractive marker pattern is exploited with respect to the axial deviation, we can probably detect the axial non-parallel tilting deviation of the upper panel. However, this modality requires further analysis with our own research in the near future.

IV. CONCLUSION

In conclusion, we have experimentally demonstrated a diffractive optic approach for analyzing the alignment between upper and lower flat panels. Using a binary DOE and affine matrix registration analysis, we have successfully shown that the lateral shift and relative rotation of axially separated panels can be analyzed with a conventional DOF limited vision camera system. With further development, the proposed diffractive alignment technique can be extended to fully three-dimensional alignment analysis of distant non-parallel panels, and can contribute to the overall enhancement of productivity and improved quality of the multilayered display manufacturing process.

FUNDING

National Research Foundation of Korea (NRF) (NRF-2019R1C1C1009988 and NRF-2022R1A2C1012559).

DISCLOSURES

The authors declare that they have no known competing financial interests or personal relationships that could have appeared to influence the work reported in this paper.

DATA AVAILABILITY

Research data are not shared.

REFERENCES

1. J.-S. Chen and D. P. Chu, “Improved layer-based method for rapid hologram generation and real-time interactive holographic display applications,” Opt. Express **23**, 18143–18155 (2015).
2. J. Geng, “Three-dimensional display technologies,” Adv. Opt. Photonics **5**, 456–535 (2013).
3. C. Chiou, F. H. Hsu, S. Petrov, V. Marinova, H. Dikov, P. Vitanov, D. Dimitrov, K. Y. Hsu, Y. H. Lin, and S. H. Lin, “Flex-

ible light valves using polymer-dispersed liquid crystals and TiO_2/Ag/TiO_2 multilayers," Opt. Express **27**, 16911–16921 (2019).
4. Y. Takaki and N. Nago, "Multi-projection of lenticular displays to construct a 256-view super multi-view display," Opt. Express **18**, 8824–8835 (2010).
5. C. Kim, J. Kim, D. Shin, J. Lee, G, Koo, and Y. H. Won, "Electrowetting Lenticular Lens for a Multi-View Autostereoscopic 3D Display," IEEE Photonics Technol. Lett. **28**, 2479–2482 (2016).
6. J. Lee, I. H. Jeong, J. H. Yu, K. H. Song, K. Jeong, S. Kang, M. Lee, and S. H. Lee, "Novel film patterned retarder utilizing in-plane electric field," Opt. Express **22**, 15315–15319 (2014).
7. D. Lee, K. Kwak, C. G. Jhun, H. S. Choi, and J. Song, "Maskless fabrication of film-patterned-retarder (FPR) using wedged liquid crystal cell," IEEE Photonics J. **11**, 7001508 (2019).
8. C. Park and S. Kwon, "An efficient vision algorithm for fast and fine mask-panel alignment," in *Proc. 2006 SICE-ICASE International Joint Conference* (Busan, Korea, Oct. 18–21, 2006), pp. 1441–1445.
9. M. V. R. K. Murty and R. P. Shukla, "Method for measurement of parallelism of optically parallel plates," Opt. Eng. **18**, 183352 (1979).
10. Y.-J. Lee, Y.-K. Kim, S. I. Jo, J. S. Gwag, C.-J. Yu, and J.-H. Kim, "Surface-controlled patterned vertical alignment mode with reactive mesogen," Opt. Express **17**, 10298–10303 (2009).
11. Y.-J. Lee, Y.-K. Kim, S. I. Jo, K.-S. Bae, B.-D. Choi, J.-H. Kim, and C.-J. Yu, "Fast vertical alignment mode with continuous multi-domains for a liquid crystal display," Opt. Express **17**, 23417–23422 (2009).
12. G. Moon, I. Son, C. Kim, C. H. Cho, E. Lee, E. H. Bae, C. Min, T. Kang, and J. H. Lee, "Fabrication of pre-tilted vertical alignment layers for high-speed liquid crystal display using bifunctional photoreactive monomers," Mol. Cryst. Liq. Cryst. **687**, 60–67 (2019).
13. I. Son, C. H. Cho, G. Moon, C. Kim, E. Lee, E. H. Bae, C. Min, T. Kang, and J. H. Lee, "A fast-switching vertically-aligned liquid crystal device based on a multi-functional mesogenic photocrosslinker," Mol. Cryst. Liq. Cryst. **687**, 68–75 (2019).
14. P. Kumar, C. Jaggi, V. Shama, and K. K. Raina, "Advancements of vertically aligned liquid crystal displays," Micron **81**, 34–47 (2016).
15. S. Jo, C. Yu, and J. Kim, "Fast response and wide viewing angle vertical alignment mode with x-shape electrode," Mol. Cryst. Liq. Cryst. **613**, 69–74 (2015).
16. N. Okaichi, M. Miura, J. Arai, M, Kawakita, and T. Mishina, "Integral 3D display using multiple LCD panels and multi-image combining optical system," Opt. Express **25**, 2805–2817 (2017).
17. Q. Wang, C. Ji, L. Li, and H. Deng, "Dual-view integral imaging 3D display by using orthogonal polarizer array and polarization switcher," Opt. Express **24**, 9–16 (2016).
18. J.-Y. Jang, D. Shin, and E.-S. Kim, "Optical three-dimensional refocusing from elemental images based on a sifting property of the periodic δ-function array in integral-imaging," Opt. Express **22**, 1533–1550 (2014).
19. H.-W. Lee, C.-H. Liu, Y.-Y. Chiu, and T.-H. Fang, "Design and control of an optical alignment system using a parallel XXY stage and four CCDs for micro pattern alignment," in *Proc. 2012 Symposium on Design, Test, Integration and Packaging of MEMS/MOEMS (DTIP)* (Cannes, France, Apr. 25–27, 2012), pp. 13–17.
20. H. Lee, D. Lee, and M. Chun, "Alignment system for display panel using edge feature," J. Korean Inst. Intell. Syst. **25**, 260–265 (2015).
21. S. Jang, W. Choi, S. Kim, J. Lee, S. Na, S. Ham, J. Park, H. Kang, B. Ju, and H. Kim, "Complex spatial light modulation capability of a dual layer in-plane switching liquid crystal panel," Sci. Rep. **12**, 8277 (2022).
22. J. Jung, B. Jeon, J. Lee, H. Ahn, Y. Shin, B. Sung, and S. Kim, "Display panel, method of manufacturing the same and alignment mask for manufacturing the same," U.S. patent US8823910B2 (2014).
23. G. Zhao and C. Lee, "Method for manufacturing alignment films of liquid crystal display panel," U. S. patent US8603287B2 (2013).
24. W. Park and M. Park, "Vision system, alignment system for aligning display panel and patterned retarder on stereoscopic image display using the vision system," U.S. patent 20120162399A1 (2012).
25. J. W. Goodman, *Introduction to Fourier Optics*, 2nd ed. (McGraw-Hill, USA, 1996).
26. H. Kim, B. Yang, and B. Lee, "Iterative Fourier transform algorithm with regularization for the optimal design of diffractive optical elements," J. Opt. Soc. Am. A **21**, 2353–2365 (2004).
27. C.-Y. Hwang, S. Oh, I.-K. Jeong, and H. Kim, "Stepwise angular spectrum method for curved surface diffraction," Opt. Express **22**, 12659–12667 (2014).
28. H. Kim, J. Kwon, and J. Hahn, "Accelerated synthesis of wide-viewing angle polygon computer-generated holograms using the interocular affine similarity of three-dimensional scenes," Opt. Express **26**, 16853–16874 (2018).
29. S. Park, J. Lee, S. Lim, M. Kim, S. Ahn, S, Hwang, S. Jeon, J. Jeong, J. Hahn, and H. Kim, "Wide-viewing full-color depthmap computer-generated holograms," Opt. Express **29**, 26793–26807 (2021).
30. H. Kim and B. Lee, "Iterative Fourier transform algorithm with adaptive regularization parameter distribution for the optimal design of diffractive optical elements," Jpn. J. Appl. Phys. **43**, L702 (2004).
31. J. Lee, J. Hahn, and H. Kim, "Diffractive-optical element for noise-reduced beam shaping of multi-array point light source," Curr. Opt. Photonics **5**, 491–499 (2021).
32. H. Kim and B. Lee, "Optimal non-monotonic convergence of iterative Fourier transform algorithm," Opt. Lett. **30**, 296–298 (2005).
33. J. Hahn, H. Kim, and B. Lee, "Optical implementation of iterative fractional Fourier transform algorithm," Opt. Express **14**, 11103–11112 (2006).